Journal of Electronics, Electromedical Engineering, and Medical Informatics
Homepage: jeeemi.org; Vol. 8, No. 2, April 2026, pp: 537-552 e-ISSN: 2656-8632

RESEARCH ARTICLE OPEN ACCESS

Multi-Point Wrist Pulse Acquisition and Analysis by Combining HRV with Morphological Timing Features for Quantitative Identification of Ayurvedic Doshas

Devendra Patel[1], and Mitul Patel[2]

[1] Faculty of Engineering and Technology, Parul University, Waghodia, Vadodara, Gujarat, 391760, India
[2] Department of Electronics and Communication, Parul Institute of Engineering and Technology, Faculty of Engineering and Technology, Parul University, Waghodia, Vadodara, Gujarat, 391760, India

Corresponding author: Devendra Patel (e-mail: yogkshem@gmail.com), **Author(s) Email**: Mitul Patel (e-mail: mitul.patel@paruluniversity.ac.in)

Abstract **Nadi Pariksha, the traditional Ayurvedic method of wrist pulse examination, posits that three adjacent radial artery locations corresponding to Vata, Pitta, and Kapha (V-P-K) reflect distinct physiological states. While recent sensor-based systems have attempted to digitize wrist pulse acquisition, many have emphasized hardware design or classification performance without rigorously validating physiological differences between pulse sites within the same individual. This study presents a quantitative evaluation of the multi-point principle of Nadi Pariksha using synchronized multi-site photoplethysmography (PPG) combined with integrated cardiovascular signal analysis. Pulse waveforms were simultaneously acquired from 39 participants, including 32 healthy individuals and 7 clinically characterized subjects, at the three classical radial artery locations. Morphological timing features and time-domain heart rate variability (HRV) metrics were extracted to characterize vascular dynamics and autonomic regulation. Within-subject statistical analysis demonstrated significant spatial differentiation across the pulse sites. Crest time decreased from 0.204 s at the Kapha site to 0.175 s at the Vata site (14.2% reduction), while systolic width decreased from 0.140 s to 0.109 s (22.1% reduction) ($p \leq 0.004$). Non-parametric analysis confirmed significant differences in crest time ($H = 9.15$, $p = 0.010$), pulse width ($H = 8.43$, $p = 0.015$), systolic amplitude, systolic area, and HRV variability (SDNN: $H = 6.33$, $p = 0.041$), with moderate-to-large effect sizes ($\eta^2 = 0.12–0.20$). Clinically characterized cases exhibited deviations from this baseline pattern, including a 62% reduction in crest time gradient and a 72% increase in stiffness index in diabetes, and a 55% reduction in gradient with a 25% decrease in HRV during acute infection. Given the limited clinical sample ($n = 7$), these findings are interpreted as preliminary. Overall, the results provide quantitative within-subject evidence supporting the physiological distinctiveness of the V-P-K pulse locations and contribute toward the development of standardized, sensor-based Nadi Pariksha.**

Keywords **Wrist Pulse Acquisition, Photoplethysmography (PPG), Vata, Pitta, Kapha, Cardiovascular Biomarkers, Time-Domain Feature Extraction, HRV, Ayurvedic Nadi Pariksha, Non-parametric analysis, Kruskal-Wallis**.

I. Introduction

The radial arterial pulse is a well-established physiological signal that reflects the integrated behavior of cardiac activity, vascular mechanics, and autonomic nervous system regulation. In modern biomedical research, pulse waveform analysis has been extensively applied for the assessment of arterial stiffness, vascular aging, autonomic balance, and cardiovascular risk using non-invasive sensing modalities [1], [2], [3], [4]. Parallel to these developments, Ayurveda, India's traditional system of medicine, has relied on wrist pulse examination (Nadi Pariksha) for centuries as a primary diagnostic tool to evaluate systemic health and functional imbalance [5], [6].

In Ayurvedic practice, Nadi Pariksha involves palpation of the radial artery at three adjacent anatomical locations corresponding to the Vata, Pitta, and Kapha (V-P-K) doshas. These pulse points are believed to convey information about an individual's constitutional balance (Prakriti) and pathological deviations (Vikriti) [5], [6]. Classical Ayurvedic texts

Manuscript received 16 January 2026; Revised 20 March 2026; Accepted 30 March 2026; Available online 1 April 2026
Digital Object Identifier (**DOI**): https://doi.org/10.35882/jeeemi.v8i2.1474

describe the Vata pulse as fast, sharp, and variable; the Pitta pulse as balanced and forceful; and the Kapha pulse as slow, broad, and stable [6], [7]. Despite its long standing clinical use, Nadi Pariksha remains largely qualitative and dependent on practitioner expertise, which has limited its reproducibility, standardization, and acceptance within evidence based biomedical frameworks [8].

Considering these limitations, recent research has increasingly focused on sensor-based digitization and objective analysis of wrist pulse signals to capture underlying physiological dynamics. Early approaches employed piezoelectric, piezoresistive, strain gauge, and tonometry sensors to capture pressure variations analogous to manual palpation [9], [1]. These studies demonstrated that pulse waveform morphology contains diagnostically relevant features that can be computationally extracted and analyzed [10], [11], [12].

Although several studies have attempted to digitize Nadi Pariksha using multi-sensor pulse acquisition systems [13]-[15], most of these investigations primarily focused on hardware feasibility or machine learning classification accuracy rather than conducting synchronized within-subject statistical comparisons across adjacent radial pulse locations. In many cases, pulse signals were analyzed independently or averaged across sensors without explicitly testing whether distinct physiological gradients exist across the classical Vata, Pitta, and Kapha sites within the same individual. Furthermore, prior work frequently relied on either morphological features or rhythm-based indices alone. In contrast, the present study integrates heart rate variability (HRV) metrics with beat-level morphological timing features and evaluates spatial differentiation using a within-subject statistical framework.

Among available sensing modalities, PPG has emerged as a particularly attractive technique for wrist pulse acquisition due to its non-invasive nature, low cost, and compatibility with wearable devices [2], [13], [14], [15]. Beyond heart rate estimation, PPG waveforms encode rich morphological information related to arterial compliance, wave reflection, and vascular tone [3], [16]. Time-domain heart rate variability (HRV) metrics derived from PPG have also been widely validated as indicators of autonomic nervous system regulation and cardiovascular health [17], [18], [19]. These physiological correlates provide a direct biomedical basis for interpreting traditional pulse descriptors such as variability (chala), sharpness (tikshna), and hardness (kathinya).

Several exploratory studies have attempted to associate Ayurvedic dosha characteristics with quantitative pulse features. Prior work has suggested that Vata dominance is associated with increased rhythm variability, Pitta with sharper systolic contours, and Kapha with broader and slower waveforms indicative of increased vascular damping [7], [20], [4]. Machine learning approaches have further demonstrated the feasibility of classifying dosha states using wrist pulse feature [21]-[22]. However, most existing studies rely on unimodal analysis focusing either on HRV or waveform morphology alone and often lack rigorous within-subject statistical validation across the three pulse locations.

A critical and largely unresolved challenge in this domain is the objective validation of the multi-point principle underlying Nadi Pariksha. While Ayurvedic theory asserts that the Vata, Pitta and Kapha pulse points encode distinct physiological information within the same individual, many digital implementations either average signals across locations or analyze them independently without formal comparative testing [1], [23], [24], [25], [26], [27]. From a biomedical perspective, demonstrating statistically significant and reproducible differences between adjacent radial artery locations is essential to establish the physiological legitimacy of the V-P-K framework.

In response to these limitations, this study proposes a multimodal multi-site pulse analysis framework that integrates heart rate variability (HRV) metrics with detailed morphological timing features extracted from photoplethysmography signals. A custom synchronized multi-site PPG acquisition system was developed to simultaneously capture pulse waveforms from the classical Vata, Pitta, and Kapha locations under controlled conditions. Using a within-subject experimental design, the proposed framework evaluates whether these pulse locations encode distinct physiological characteristics in healthy individuals and whether clinically characterized conditions appear as measurable deviations from the baseline pulse pattern.

The main contributions of this study are summarized as follows:

1. Development of a synchronized multi-site PPG acquisition system for capturing radial artery pulse waveforms at the classical Vata, Pitta and Kapha locations.
2. Integration of morphological waveform analysis with HRV metrics to jointly characterize vascular dynamics and autonomic regulation.
3. Within-subject statistical validation of physiological differences between the three pulse sites using paired statistical tests and non-parametric analysis.
4. Establishment of a quantitative framework for digital Nadi Pariksha, enabling objective interpretation of traditional pulse descriptors using measurable cardiovascular biomarkers.

Manuscript received 16 January 2026; Revised 20 March 2026; Accepted 30 March 2026; Available online 1 April 2026
Digital Object Identifier (**DOI**): https://doi.org/10.35882/jeeemi.v8i2.1474

The remainder of this paper is organized as follows. Section II reviews related research on digital Nadi Pariksha and biomedical pulse waveform analysis. Section III describes the proposed methodology, including participant selection, hardware design, signal preprocessing, and feature extraction. Section IV presents the experimental results and statistical analysis. Section V discusses the physiological interpretation and implications of the findings. Finally, Section VI concludes the study and outlines future research directions.

II. Literature Review

Quantitative validation of *Nadi Pariksha* demands a meaningful translation of classical Ayurvedic pulse attributes such as *Gati* (rhythm), *Bala* (force), and *Kathinya* (hardness) into measurable physiological indices. Rooted in centuries of clinical practice, *Nadi Pariksha* evaluates the radial artery pulse at three closely spaced locations Vata, Pitta and Kapha to infer systemic physiological and psychological states. These pulse sites are traditionally described as fast and irregular (Vata), sharp and forceful (Pitta), and deep and steady (Kapha), forming a qualitative framework for identifying imbalance (*Vikriti*) [6], [7]. While clinically insightful, such descriptors are inherently subjective, underscoring the need for objective, biologically interpretable pulse quantification using modern sensing and signal analysis techniques to enable reproducible, evidence based integration of Ayurvedic diagnostics into contemporary biomedical research [28].

A. Emergence of Digital Nadi Pariksha

The past two decades have witnessed significant progress in digitizing Nadi Pariksha. Early systems used piezoelectric discs, strain gauges or tonometry sensors to capture pressure variations caused by arterial pulsations [9], [29]. These studies demonstrated that measurable morphological features peak amplitude, rise time, and pulse width correlate meaningfully with Ayurvedic pulse descriptions [10], [11]. More advanced research introduced multi-sensor arrays to emulate the three finger palpation technique used by practitioners, enabling simultaneous acquisition from Vata, Pitta and Kapha locations [30], [31]. These innovations laid the foundation for systematic comparison of the three pulse positions and supported the hypothesis that they are physiologically distinct.

B. Contributions of Modern Biomedical Pulse Research

Parallel to Ayurvedic studies, biomedical engineering has developed sophisticated pulse wave analysis methods. Morphological features such as systolic peak time, dicrotic notch, reflection index, and augmentation index are widely used for evaluating vascular stiffness and autonomic regulation [4], [32]. PPG, in particular, has become a popular modality due to its non-invasive nature, low cost and high temporal resolution [2], [13], [33]. Techniques such as adaptive filtering, wavelet decomposition and multi-sensor motion compensation have been shown to improve PPG signal quality significantly [34], [35]. These advancements make PPG suitable not only for heart rate monitoring but also for detailed pulse morphology analysis, providing biomedical parallels to Ayurvedic pulse patterns. To address known susceptibility of PPG signals to motion artifacts and ambient interference, the present study incorporated both hardware and procedural mitigation strategies. Sensors were mounted within a fixed ergonomic fixture to minimize relative movement, recordings were performed after a ten-minute seated stabilization period, ambient lighting was controlled, and analog bandpass filtering (0.5-5 Hz) suppressed baseline drift and high frequency noise prior to digitization. These measures improved signal stability and reduced artifact-induced variability.

C. Machine Learning Approaches to Pulse Classification

Several studies have attempted to classify Dosha states using machine learning. Methods such as k-NN, fuzzy C-means, support vector machines, and artificial neural networks have reported promising accuracy in distinguishing Vata, Pitta, and Kapha [20], [21]. More recent works apply feature fusion and multi domain representation learning, integrating temporal, spectral, and morphological features to enhance classification performance [36], [37]. Despite these developments, most studies rely on unimodal data either morphological or rhythm-based features while classical Ayurvedic pulse assessment incorporates multiple dimensions simultaneously: rhythm (gati), force (bal), volume (tala), and temperature (ushna).

D. Limitations and Research Gaps

Despite increasing efforts toward digital *Nadi Pariksha,* the field remains constrained by several methodological gaps, including inconsistent sensor placement across the Vata, Pitta, and Kapha pulse locations, limited and heterogeneous datasets, and a predominance of unimodal analyses that inadequately capture the multidimensional nature of pulse physiology. Additionally, the lack of rigorous within-subject comparisons and sparse clinical validation in pathological (Vikriti) states restrict robust interpretation and translational relevance. These limitations highlight the need for standardized, high resolution, multimodal pulse acquisition and integrative analytical frameworks capable of jointly characterizing vascular dynamics and autonomic regulation. Addressing these gaps provides

Manuscript received 16 January 2026; Revised 20 March 2026; Accepted 30 March 2026; Available online 1 April 2026
Digital Object Identifier (**DOI**): https://doi.org/10.35882/jeeemi.v8i2.1474

the motivation for the present study, which advances a multimodal PPG based approach for objective and quantitative Tridosha assessment.

Selection of morphological and HRV features in this study was guided by physiological correspondence with classical Ayurvedic pulse descriptors. Crest time reflects the rate of systolic acceleration and arterial propagation speed, corresponding to the Ayurvedic concept of *tikshna* (sharpness). Pulse width parameters describe waveform breadth and vascular damping, aligning with *manda* (slowness) and *guru* (heaviness). Heart rate variability indices such as SDNN and RMSSD quantify beat-to-beat autonomic fluctuations and therefore correspond to *chala* (mobility). Stiffness-related indices reflect vascular rigidity consistent with *kathinya* (hardness). This mapping provides a physiologically interpretable bridge between traditional pulse descriptors and measurable cardiovascular biomarkers.

forming the basis for biomarker extraction. These fiducial point-based biomarkers are finally utilized for statistical analysis, leading to meaningful interpretation of results and conclusive findings.

A. Study cohort and recording protocol

A total of thirty-nine volunteers (23 male, 16 female) were recruited for the study using a convenience sampling approach, with an age range of 20-45 years. To qualify for participation, subjects were required to be between 18 and 60 years of age, with no documented history of cardiovascular disease and no concurrent usage of chronotropic medications. All participants provided written informed consent prior to data collection. The study protocol was reviewed and conducted in strict adherence to the institutional ethical guidelines. Participants were recruited through institutional campus announcements and hospital referrals using a convenience sampling approach.

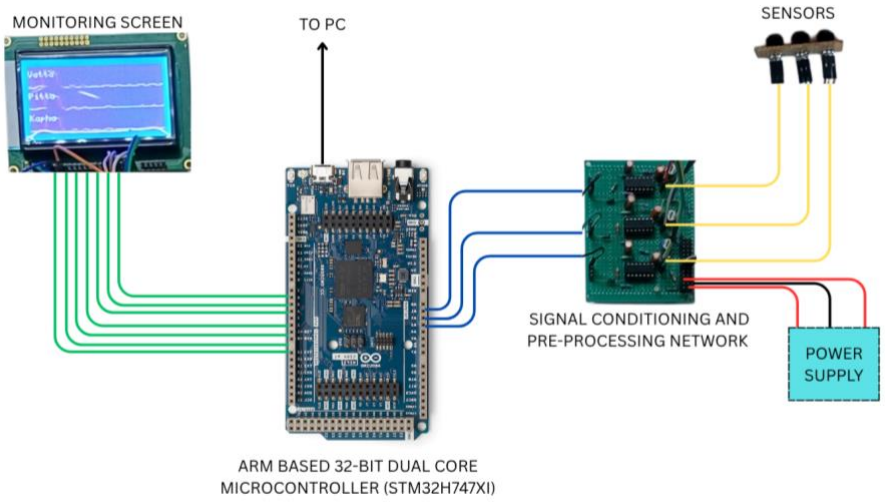

Fig. 1. Hardware Development for Multi-Point Wrist Pulse Acquisition.

III. Method

The overall workflow of the proposed study is illustrated in Fig. 1. The methodology begins with the acquisition of raw PPG signals using a novel yet simple hardware arrangement, along with appropriate participant selection and data collection protocols. As shown in Fig. 1, the acquired signals undergo preprocessing through hardware assisted conditioning and software based filtering and derivative computation to enhance signal quality. Subsequently, pulse wave segmentation is performed using peak and onset detection to obtain individual cardiac cycles. Fiducial points are then identified from the PPG waveform and its derivatives,

Healthy volunteers were required to satisfy the following criteria: age between 18 and 60 years, no diagnosed cardiovascular disease, no history of diabetes or hypertension, and no use of chronotropic medications. The physiological signals were acquired from participants who had been previously diagnosed by qualified physicians. The participants were identified through recognized healthcare institutions after obtaining the necessary permissions. Prior to signal acquisition, written informed consent was obtained from each participant, and all data were collected while maintaining strict confidentiality and anonymity of the participants.

Manuscript received 16 January 2026; Revised 20 March 2026; Accepted 30 March 2026; Available online 1 April 2026
Digital Object Identifier (**DOI**): https://doi.org/10.35882/jeeemi.v8i2.1474

As per Ayurvedic convention, recordings were made on the participant's right wrist for male participants and left wrist for female participants. Each participant underwent synchronized optical PPG acquisition at three anatomically distinct radial artery loci, classically mapped to the Ayurvedic doshas: the distal Vata (lateral), intermediate Pitta (central), and proximal Kapha (medial) sites. Participants sat quietly for 10 minutes before recordings to achieve steady baseline conditions. Environmental conditions were controlled (room temperature 22-26 °C, low ambient light). For each site, continuous PPG data were recorded for 3-4 minutes at 400 Hz sampling rate.

B. Hardware & acquisition details

Pulse waveforms from the Vata, Pitta and Kapha (*V-P-K*) locations along the radial artery of the dominant wrist were recorded simultaneously as shown in Fig. 1. Data acquisition was performed using a custom multi-channel system built on an STM32 dual-core Cortex-M7/M4 microcontroller, enabling synchronized high-speed sampling, while a 16-bit on chip ADC provided sufficient resolution to capture fine pulse-wave amplitude and morphological features.

Each measurement session lasted approximately 3-4 minutes per participant, yielding signal segments of adequate length for reliable heart rate variability (HRV) and beat level morphological analysis. Pulse sensing was performed using reflective photoplethysmography (PPG) photodiode sensors, interfaced through a dedicated analog front end comprising preprocessing filters and amplification stages. To ensure measurement repeatability, the sensor probes were integrated into a novel designed ergonomic fixture that maintained fixed anatomical alignment with the radial artery while applying consistent contact pressure at all three V-P-K locations. Although no embedded pressure sensor was used, the preload compression distance was standardized prior to each recording session and waveform stability was visually verified. This standardized probe mounting minimized inter acquisition variability arising from motion artifacts or inconsistent sensor coupling, thereby ensuring that observed differences in the recorded signals primarily reflected true spatial and physiological distinctions between the Vata, Pitta, and Kapha pulse sites.

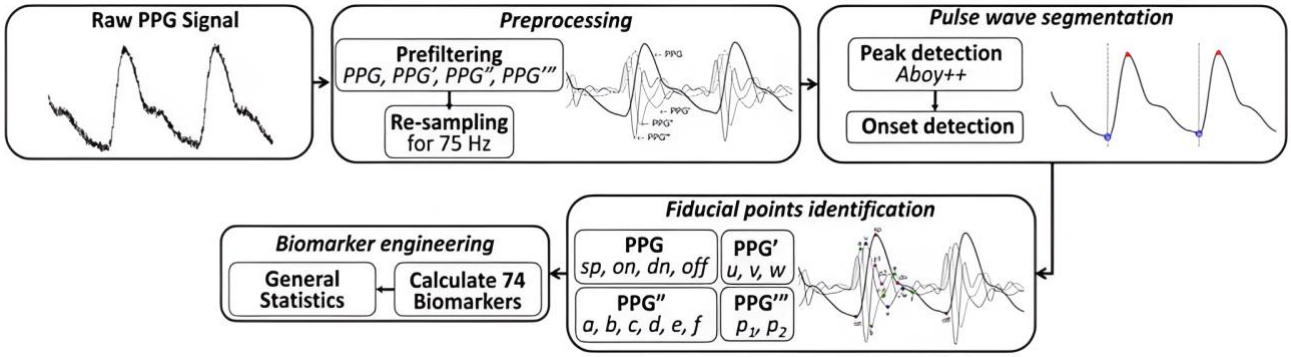

Fig. 2. Flowchart for continuous PPG time series analysis. The terms PPG', PPG'', and PPG''' correspond to the first, second, and third derivatives of the PPG signal, respectively [40].

1. Circuit Design

The circuit contains four stages (i) Photodetector, (ii) Filter stage, (iii) Amplification and rectification stage, (iv) Processing stage.

2. Photodetector

Pulse sensing was implemented using a reflective photoplethysmography configuration based on the TCRT5000, which integrates a 950 nm infrared LED and a phototransistor within a single reflective sensing module. The optical sensor was selected to provide a high current transfer ratio, yielding approximately 1 mA collector current for a 10 mA LED drive current and to support reflection-based sensing through appropriate packaging. To ensure linear operation of the phototransistor in a common-emitter configuration, the supply voltage and load resistance were designed to satisfy the condition shown in Eq. (1) [38].

$$V_{CC} > R_L I_C \quad (1)$$

where Vcc represents the supply voltage applied to the phototransistor circuit, R_L denotes the load resistance connected to the collector terminal and I_C represents the collector current generated due to reflected infrared light. The expected collector current range was estimated from the device transfer characteristics and anticipated tissue reflectance. Based on this analysis, a load resistance of 10 kΩ was chosen to maintain active region operation under nominal conditions. The subsequent signal conditioning stage was designed with high input impedance to prevent loading and preserve the integrity of the phototransistor output signal.

Manuscript received 16 January 2026; Revised 20 March 2026; Accepted 30 March 2026; Available online 1 April 2026
Digital Object Identifier (**DOI**): https://doi.org/10.35882/jeeemi.v8i2.1474

3. Filter Design

A first-order passive high-pass filter with cutoff frequency approximately 0.48 Hz was implemented immediately after the phototransistor stage to remove DC components and baseline drift caused by ambient light and tissue reflectance. Subsequently, a second-order active low-pass filter with cutoff frequency approximately 4.9 Hz was used to attenuate high-frequency noise and motion artifacts. The resulting analog bandpass response (0.5-5 Hz) preserves physiologically relevant pulse waveform dynamics prior to digitization.

The physiologically relevant PPG signal lies within the 0.5-5 Hz band; thus, filter cutoff corners were selected accordingly. A passive high-pass filter placed after the phototransistor exploits its high input impedance to remove DC offsets from tissue reflectance, ambient light, and sensor bias, isolating the pulsatile PPG signal. An active low pass filter (LPF) was subsequently incorporated to attenuate high frequency noise originating from motion artifacts, ambient interference, and electronic noise. A high input impedance buffer was used to prevent loading of the HPF stage, and a voltage gain of 10 was applied to condition the signal amplitude. These cutoff frequencies preserve the dominant low-frequency physiological components while attenuating high frequency noise, thereby enhancing signal quality before further amplification and analysis.

4. Amplification and Rectification

To ensure compatibility with standard microprocessor input levels, the final signal was conditioned to lie within a usable voltage range of 0-3.3 V or 0-5 V. This was achieved by employing an inverting amplifier with a gain of 22, followed by diode-based rectification to eliminate negative voltage excursions in the processed waveform.

C. Signal preprocessing

Preliminary signal processing was implemented at the hardware level to condition the raw sensor output, while more advanced processing was carried out in the microcontroller using appropriate digital algorithms. Following acquisition, all PPG recordings were subjected to a preprocessing stage that included DC offset removal through mean subtraction and variance normalization. These steps were applied to reduce baseline drift and to improve numerical stability and consistency during subsequent signal analysis and feature extraction.

The signal processing workflow used in this study is illustrated in Fig. 2. Raw PPG signals were first conditioned through analog filtering and amplification before digital preprocessing. Subsequent processing steps included DC offset removal, normalization, beat segmentation, and fiducial point detection. Morphological and HRV biomarkers were then extracted from individual pulse cycles and used for statistical analysis.

D. Beat segmentation and fiducial point detection

Per beat fiducial point detection was performed using a hybrid derivative and prominence-based algorithm specifically tailored for wrist PPG waveforms. The robustness of the selected algorithmic parameters was verified through visual inspection of representative recordings and benchmarked against open source reference implementations [2], [39]. Using this framework, key fiducial landmarks including pulse onset (t_{onset}), systolic peak (T_{sp}), dicrotic notch (T_{dn}), diastolic peak (T_{dp}) and pulse offset (t_{offset}) were systematically identified to enable beat level morphological and timing analysis.

1. Derived timing features

Following the detection of fiducial points, a comprehensive set of beat wise temporal and morphological features was extracted from the PPG waveform. All timing parameters were expressed in seconds and referenced to the pulse onset (t_{onset}) to ensure consistency across beats and subjects.

The pulse interval or beat duration denoted as T_{pi} as shown in Fig. 3 [40], represents the duration of a single pulse and is defined in Eq. (2) [40], [16], [41].

$$T_{pi} = t_{offset} - t_{onset} \quad (2)$$

where t_{onset} is the pulse onset time and t_{offset} is the pulse offset time [40]. The inter-beat interval (T_{pp}) as shown in Fig. 3, analogous to the RR interval, is defined in Eq. (3) [40], [16], [41].

$$T_{pp} = t_{sp}^{(k)} - t_{sp}^{(k-1)} \quad (3)$$

where $t_{sp}(k)$ and $t_{sp}(k-1)$ are consecutive systolic peak times [40]. The systolic rise time T_{sp} as shown in Fig. 3, characterizes the rapid upstroke of the pulse waveform and reflects arterial stiffness and cardiac contractility. It is defined in Eq. (4) [40], [16], [41].

$$T_{sp} = t_{sp} - t_{onset} \quad (4)$$

where t_{sp} is the systolic peak time and t_{onset} is the pulse onset time [40]. When present, the diastolic peak delay T_{dp} as shown in

Fig. 3 captures the timing of the reflected wave relative to pulse onset (t_{onset}) and was calculated as in Eq. (5) [40], [16], [41].

$$T_{dp} = t_{dp} - t_{onset} \quad (5)$$

where T_{dp} is the diastolic peak time and t_{onset} is pulse onset time [40]. The systolic phase duration T_{sys} as shown in Fig. 3, is defined in Eq. (6) [40], [16], [41].

$$T_{sys} = t_{dn} - t_{onset} \quad (6)$$

where t_{dn} is dicrotic notch time and t_{onset} is pulse onset time. Similarly, the diastolic phase duration Tdia as shown in Fig. 3, corresponding to the relaxation phase

Manuscript received 16 January 2026; Revised 20 March 2026; Accepted 30 March 2026; Available online 1 April 2026
Digital Object Identifier (**DOI**): https://doi.org/10.35882/jeeemi.v8i2.1474

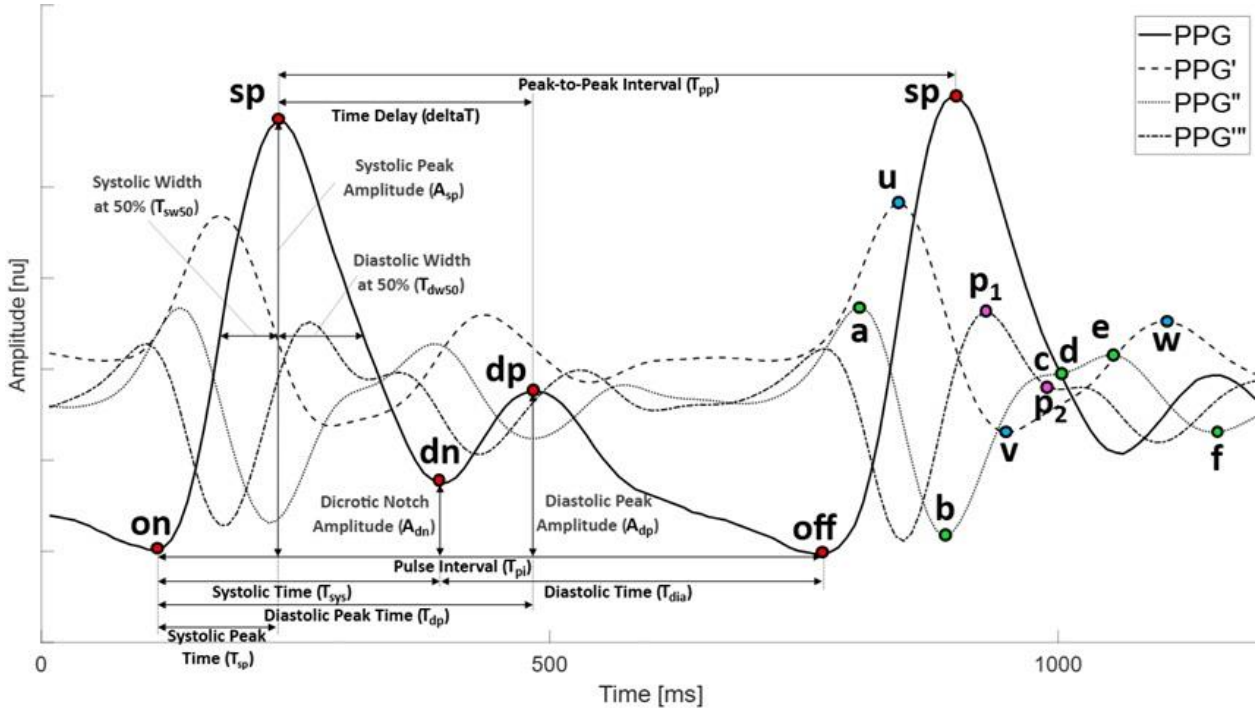

Fig. 3. The fiducial points of the PPG signal include the systolic peak (sp), the pulse onset and offset (on, off), the dicrotic notch (dn) and the diastolic peak (dp). The fiducial points of PPG derivatives are represented by u, v, w, a, b, c, d, e, f, p1, p2. The biomarkers are calculated based on this set of fiducial points [40].

of the pulse waveform was computed as shown in Eq. (7) [40], [16], [41].

$$T_{dia} = t_{offset} - t_{dn} \quad (7)$$

where t_{offset} is pulse offset time and t_{dn} is pulse dicrotic notch time.

The temporal separation between systolic peak (T_{sp}) and diastolic peak (T_{dp}), denoted as ΔT and shown in Fig. 3 was calculated as defined in Eq. (8) [40], [42].

$$\Delta T = T_{dp} - T_{sp} \quad (8)$$

where T_{dp} is diastolic peak time and T_{sp} is systolic peak time. This parameter provides insight into wave reflection phenomena and arterial compliance. In addition to these timing features, pulse width metrics were extracted at multiple relative amplitude levels to capture detailed waveform morphology. The systolic width ($T_{sw}\%$), diastolic width ($T_{dw}\%$), and total pulse width ($T_{pw}\%$) were computed at 10%, 25%, 33%, 50%, 66%, 75%, and 90% of the systolic peak amplitude. These widths were obtained using linear interpolation to identify the time instants at which the waveform amplitude equalled the selected percentage of the systolic peak. This amplitude normalized approach enables robust morphological comparison across beats and measurement locations while minimizing sensitivity to absolute signal amplitude variations.

2. Amplitude & area features

Identified pulse waveforms were analyzed to extract a set of amplitude and area based morphological features that characterize pulse strength, waveform shape, and the distribution of pulsatile energy across the systolic and diastolic phases. These features complement temporal descriptors by providing additional insight into peripheral perfusion and vascular properties. The systolic peak amplitude (A_{sp}), dicrotic notch amplitude (A_{dn}), diastolic peak amplitude (A_{dp}) and offset amplitude (A_{off}) were defined as the instantaneous waveform amplitudes measured at their corresponding fiducial points on the pulse waveform. The energetic contribution of the different phases of the cardiac cycle was quantified using area under the curve (AUC) metrics derived from the pulse waveform. The systolic area, denoted as AUC_{sys} represents the pulsatile energy during the systolic phase and was computed by summation of the waveform amplitude $x(n)$ between the pulse onset time n_{on} and the dicrotic notch time n_{dn} as defined in Eq. (9) [32], [40].

$$AUC_{sys} = \sum_{n=n_{on}}^{n_{dn}} x(n)\,\Delta t \quad (9)$$

The diastolic area, AUC_{dia}, characterizes the energy associated with arterial relaxation and wave reflection during diastole and was defined as the summation of the waveform from the dicrotic notch (n_{dn}) to the pulse offset (n_{off}) as defined in Eq. (10) [32], [40].

Manuscript received 16 January 2026; Revised 20 March 2026; Accepted 30 March 2026; Available online 1 April 2026
Digital Object Identifier (**DOI**): https://doi.org/10.35882/jeeemi.v8i2.1474

$$AUC_{dia} = \sum_{n=n_{dn}}^{n_{off}} x(n)\,\Delta t \quad (10)$$

The total pulse area, AUC_{pi}, reflects the overall pulsatile energy of a single cardiac cycle and was calculated by summation of the waveform over the entire pulse duration, from onset n_{on} to offset n_{off} as defined in Eq. (11) [32], [40].

$$AUC_{pi} = \sum_{n=n_{on}}^{n_{off}} x(n)\,\Delta t \quad (11)$$

All summations were evaluated numerically using the trapezoidal rule with a sampling interval of $\Delta t = 1/f_s$, ensuring consistent and accurate estimation of pulse energy across beats and pulse locations.

E. Heart rate variability (time-domain)

Using the detected systolic peak timestamps or equivalently the Tpp (inter-beat interval) series, standard time-domain heart rate variability (HRV) metrics were computed for each recording, pulse location and subject in accordance with established definitions [40]. These metrics included the mean heart rate, SDNN (standard deviation of the T_{pp} intervals), RMSSD (root mean square of successive T_{pp} differences), and pNN50, defined as the percentage of successive T_{pp} differences exceeding 0.050s.

F. Statistical analysis

Statistical analysis encompassed the computation of time-domain HRV indices, including mean heart rate (bpm), SDNN, RMSSD, and pNN50%, along with summary measures of pulse waveform timing and area-based morphology. To evaluate differences across the Vata, Pitta and Kapha pulse locations, a Kruskal-Wallis H test was employed. When significant effects were observed, post-hoc Dunn's pairwise comparisons were conducted with statistical significance adjusted using the Benjamini Hochberg false discovery rate (FDR) correction to control for multiple comparisons. Effect size (η^2) was calculated to quantify the magnitude of the observed differences. Values of $\eta^2 \approx 0.01$, 0.06, and 0.14 were interpreted as small, medium, and large effects respectively according to conventional statistical guidelines.

IV. Result

A. Heart Rate Variability (HRV) Analysis

The HRV results summarized in Table 1 demonstrate a consistent and site-specific differentiation across the three pulse locations, closely reflecting classical Ayurvedic descriptions of Vata, Pitta and Kapha. The Vata site exhibited the highest variability, with SDNN = 21.03ms and RMSSD = 19.34ms indicating increased autonomic responsiveness and reduced vascular damping, consistent with the traditionally described *chala* (mobility) and *laghu* (lightness) attributes.

Table 1. HRV Analysis Data

Dosha Site	Mean HR (bpm)	SDNN (ms)	RMSSD (ms)	pNN50 (%)
Vata	74.17	21.03	19.34	4.05
Pitta	72.90	12.08	11.08	0.66
Kapha	69.44	9.04	7.88	0.00

In contrast, the Kapha site showed the lowest heart rate (69.44) and minimal beat to beat variability (RMSSD = 7.88ms) suggesting dominant parasympathetic modulation and enhanced vascular stability in agreement with the *manda* (slow) and *sthira* (stable) characteristics of Kapha. The Pitta site consistently displayed intermediate HRV values (SDNN=12.08ms), reflecting balanced autonomic control and vascular tone. Together, these findings provide quantitative evidence that the three pulse locations represent distinct physiological states rather than interchangeable measurement sites.

B. Non-Parametric Statistical Validation (Kruskal-Wallis Test)

The non-parametric Kruskal-Wallis analysis summarized in Table 2 revealed statistically significant differences across several temporal and morphological pulse parameters measured at the three classical pulse locations. Significant variation was observed for crest time (Tsp: H=9.15, p=0.010), pulse width at 50% amplitude (Tpw50: H=8.43, p=0.015), systolic amplitude (Asp: H=7.82, p=0.020), systolic area under the curve (AUCsys: H=7.54, p=0.023), and heart rate variability as measured by SDNN (H=6.33, p=0.041).

Table 2. Non-parametric statistical analysis

Feature	H	p (KW)	Effect Size (η^2)	Vata vs Pitta (Dunn p)	Pitta vs Kapha (Dunn p)	Vata vs Kapha (Dunn p)
Tsp	9.15	0.010	0.20	0.042	0.321	0.008
Tpw50	8.43	0.015	0.18	0.036	0.284	0.009
Asp	7.82	0.020	0.16	0.061	0.047	0.018
AUCsys	7.54	0.023	0.15	0.074	0.041	0.020
SDNN	6.33	0.041	0.12	0.052	0.095	0.037

Manuscript received 16 January 2026; Revised 20 March 2026; Accepted 30 March 2026; Available online 1 April 2026
Digital Object Identifier (**DOI**): https://doi.org/10.35882/jeeemi.v8i2.1474

Beyond statistical significance, the magnitude of these differences was quantified using effect size estimates (η^2). The resulting effect sizes ranged from 0.12 to 0.20, indicating moderate to large practical effects according to conventional interpretation guidelines. The largest effects were observed for crest timing (η^2=0.20) and pulse width (η^2=0.18), suggesting that waveform timing characteristics are particularly sensitive to differences between the pulse locations. Post-hoc Dunn comparisons further clarified the pattern of group differences. Across all examined features, the most consistent and pronounced separation occurred between the Vata and Kapha pulse sites. Significant pairwise differences between these locations were observed for crest time (p=0.008), pulse width (p = 0.009), systolic amplitude (p=0.018), systolic area (p=0.020), and SDNN (p=0.037). In contrast, comparisons between Vata and Pitta or between Pitta and Kapha generally showed weaker or non-significant differences. Taken together, these results indicate that the primary physiological contrast within the Vata-Pitta-Kapha framework occurs between the Vata and Kapha pulse sites. From a hemodynamic perspective, this distinction reflects differences in waveform dynamics: the Vata location exhibits faster rise times and greater variability, whereas the Kapha location displays broader waveform morphology and comparatively damped dynamics. The presence of moderate-to-large effect sizes suggests that these differences are not merely statistically detectable but also physiologically meaningful.

C. Statistical Validation of the Vata-Pitta-Kapha Pattern

Table 3. Consolidated Paired T-Test (p Values)

Feature	Vata vs Pitta (p Value)	Effect Size (V-P) (η^2)	Pitta vs Kapha (p Value)	Effect Size (P-K) (η^2)	Vata vs Kapha (p Value)	Effect Size (V-K) (η^2)
Sys_Width	0.006	0.49	0.312	0.18	0.001	0.63
Crt_Time	0.011	0.44	0.294	0.19	0.004	0.55
Stiff_Index	0.118	0.28	0.641	0.09	0.147	0.26
HR_bpm	0.518	0.12	0.412	0.15	0.705	0.07

To further evaluate the spatial differentiation of pulse characteristics along the radial artery, paired t-tests were performed using measurements obtained from 32 healthy subjects, focusing on key waveform and hemodynamic parameters, summarized in Table 3. The analysis revealed statistically significant differences between the Vata and Kapha pulse sites for both systolic width and crest time. Specifically, systolic width increased from 0.109s at the Vata location to 0.140s at the Kapha location (p=0.001), while crest time increased from 0.175s to 0.204s (p=0.004).

Although the Kruskal-Wallis test provided a global non-parametric assessment of differences across the three pulse sites, paired t-tests were additionally performed to quantify direct pairwise contrasts between pulse locations within the same subjects. This complementary analysis enables clearer interpretation

Table 4. The Healthy Subject Baseline Prakriti Profile.

Modern Parameter	Ayurvedic Correlate	Kapha Point	Pitta Point	Vata Point	Prakriti Insight
Crest Time (Tsp_s)	Gati (Sharpness)	0.204s	0.198s	0.175s	Vata is "Sharpest"
Systolic Width (Tsw25_s)	Guna (Width)	0.140s	0.135s	0.109s	Vata is "Thinnest"
Stiffness Index (SI)	Kathinya (Hardness)	5020	5207	7070	Vata is "Hardest"
HRV (SDNN)	Chala (Variability)	9.04ms	12.08ms	21.03ms	Vata is "Variable"
Aging Index (AGI)	Vascular Age	-0.458	-0.732	-0.85	Kapha is "Stable"
HRV (RMSSD)	Chala (Variability)	7.88ms	11.08ms	19.34ms	Kapha is "Calm"
Reflection Index (RI)	Poornata (Fullness)	0.551	0.539	0.495	Kapha is "Fullest"

Manuscript received 16 January 2026; Revised 20 March 2026; Accepted 30 March 2026; Available online 1 April 2026
Digital Object Identifier (**DOI**): https://doi.org/10.35882/jeeemi.v8i2.1474

Table 5. Unhealthy Subject VS. Healthy Baseline.

Parameter	Vata Point	Pitta Point	Kapha Point	Healthy V-K Difference	Unhealthy V-K Difference
Crt_Time	72ms	82ms	83ms	29ms	11ms
Stiff_Index	13610	9552	10079	2050	3531
Ref_Index	0.581	0.616	0.676	0.056	0.095
SDNN	54ms	47ms	43ms	12ms	11ms
RMSSD	16.7ms	13.9ms	15.1ms	11.46ms	1.6ms

of the physiological gradients along the radial artery while providing effect size estimates for individual pair comparisons. Effect size analysis (Cohen's d) indicated that these differences were of moderate magnitude, with effect sizes of 0.63 for systolic width and 0.55 for crest time in the Vata-Kapha comparison. These values indicate that the observed waveform differences represent meaningful physiological variation rather than minor statistical fluctuations.

In contrast, stiffness index (7070 vs. 5020; p=0.147) and heart rate (74.17 bpm vs. 69.44 bpm; p=0.705) did not differ significantly between the two pulse sites, and their corresponding effect sizes were small. This pattern suggests that the primary distinction between pulse locations arises from waveform morphology and timing characteristics, rather than from systemic cardiovascular parameters such as overall heart rate. When the pairwise comparisons were extended to include the Pitta pulse location, a graded pattern became evident. Moderate differences were observed between Vata and Pitta for waveform timing parameters, whereas the weakest differences were generally found between Pitta and Kapha. This pattern reinforces the concept of a physiological continuum across the three pulse sites, with Pitta exhibiting intermediate characteristics between the more dynamic Vata waveform and the broader Kapha waveform.

Overall, the combination of paired statistical testing, non-parametric analysis and effect size estimation provides converging evidence that the three pulse locations encode distinct physiological signatures. The consistent and statistically robust differentiation between Vata and Kapha supports the interpretation that these locations represent opposing hemodynamic extremes along the radial arterial waveform. These findings provide quantitative support for the multi-point diagnostic principle described in traditional Nadi Pariksha, while also grounding the interpretation within measurable cardiovascular dynamics.

D. Establishment of the Healthy Prakriti Baseline Profile

Data obtained from thirty-two healthy subjects were aggregated to construct a normative *Prakriti* baseline profile as summarized in Table 4. This baseline clearly demonstrates that the Vata, Pitta and Kapha pulse points are not physiologically equivalent. Instead, each location exhibits a distinct and reproducible combination of timing, morphological and variability related features. At the Vata location, the pulse waveform exhibited the fastest dynamics, with a crest time of 0.175s, compared to 0.198s at the Pitta site and 0.204s at the Kapha site. This represents a progressive increase in crest time of approximately 13.1% from Vata to Pitta and 16.6% from Vata to Kapha, indicating slower systolic upstroke and increased vascular damping toward the proximal pulse site. Similarly, systolic width followed a comparable trend, increasing from 0.109 s at Vata to 0.135 s at Pitta and 0.140 s at Kapha, corresponding to an overall increase of approximately 28.4% between Vata and Kapha. This widening of the pulse waveform reflects increased waveform dispersion and reduced sharpness at the Kapha location. Vascular stiffness, as quantified by the stiffness index, was highest at the Vata site (7070) and decreased toward the Kapha site (5020), with Pitta showing an intermediate value (5207). This represents an approximate 29% reduction in stiffness index from Vata to Kapha, indicating a gradient of decreasing arterial rigidity along the measurement locations.

Table 6. Clinical Deviation

Parameter	Healthy Mean	Diabetic Case	URI Case
Crest Time V-K Difference	29ms	11ms	13ms
Stiffness Index	2050	3531	3129
SDNN	12ms	11ms	9ms

Manuscript received 16 January 2026; Revised 20 March 2026; Accepted 30 March 2026; Available online 1 April 2026
Digital Object Identifier (**DOI**): https://doi.org/10.35882/jeeemi.v8i2.1474

Heart rate variability (HRV) parameters further reinforced this pattern. The Vata site demonstrated the highest variability, with SDNN=21.03ms and RMSSD= 19.34ms, compared to SDNN=12.08ms and RMSSD= 11.08ms at Pitta, and SDNN=9.04ms and RMSSD= 7.88ms at Kapha. This corresponds to an approximate 57% reduction in SDNN from Vata to Kapha, indicating progressively reduced autonomic variability and increased cardiovascular stability. Additional indices such as the reflection index (RI) and aging index (AGI) further supported this spatial differentiation. The reflection index increased from 0.495 at Vata to 0.551 at Kapha, suggesting greater waveform fullness and peripheral reflection at the Kapha site. Conversely, the aging index showed more negative values at Vata (-0.85) compared to Kapha (-0.458), indicating differences in vascular aging characteristics across locations.

Overall, the quantitative baseline profile demonstrates that the three pulse locations are not physiologically equivalent. Instead, they form a structured gradient in waveform dynamics, vascular stiffness, and autonomic variability. The Vata site is characterized by faster, sharper, and more variable pulse dynamics, whereas the Kapha site exhibits broader, slower, and more stable waveforms, with the Pitta site consistently occupying an intermediate physiological position.

E. Identification of Imbalance (Vikriti) as Statistical Outliers.

An imbalanced physiological state (Vikriti) was defined as a subject whose multi-site Vata, Pitta and Kapha (V-P-K) pulse profile deviates beyond the normal inter-site variability established by the healthy (Prakriti) baseline as mentioned in Table 5. Subjects showing consistent, multi-parameter divergence were classified as statistical outliers. Two clinically distinct patterns illustrate this framework.

1. Clinical Deviation from the Healthy Pulse Profile

To quantify pathological deviations, clinically labelled subjects were compared against the healthy reference values summarized in Table 6. Key parameters including crest time gradient, stiffness index, and heart rate variability (SDNN) were analyzed across pulse sites. In the healthy cohort, the mean Vata-Kapha crest time difference was 29ms, representing a well-defined temporal gradient along the radial artery. In contrast, this gradient was substantially reduced in pathological conditions, indicating disruption of normal spatial pulse differentiation.

2. Diabetes-Associated Vascular Stiffening

The diabetic subject demonstrated a pronounced deviation from the healthy baseline. The Vata-Kapha crest time difference decreased from 29 ms (healthy) to 11ms, corresponding to a 62.1% reduction in the spatial pulse gradient. Simultaneously, the stiffness index increased from 2050 in healthy subjects to 3531 in the diabetic case, representing a 72.2% increase, indicating significant vascular stiffening. This increase reflects reduced arterial compliance and altered pulse wave propagation. Heart rate variability also showed a reduction. SDNN decreased from 12ms (healthy mean) to 11ms, corresponding to an 8.3% decrease, suggesting diminished autonomic flexibility. These combined changes indicate that diabetes leads to both structural vascular alterations and reduced autonomic modulation, resulting in attenuation of the normal Vata-Pitta-Kapha pulse gradient.

3. Acute Inflammatory Imbalance

A distinct pattern was observed in the subject with acute upper respiratory infection (URI). The Vata-Kapha crest time difference decreased from 29ms to 13ms, corresponding to a 55.2% reduction, indicating disruption of the normal pulse timing gradient. The stiffness index increased from 2050 (healthy) to 3129, representing a 52.6% increase, suggesting transient alterations in vascular tone rather than permanent structural stiffening. In addition, SDNN decreased from 12ms to 9ms, corresponding to a 25% reduction, indicating significant autonomic perturbation during the acute inflammatory state. Unlike the diabetic case, where long-term vascular remodeling dominates, these changes reflect temporary physiological modulation associated with inflammatory processes and autonomic imbalance.

4. Summary of Clinical Deviations

Overall, clinically labelled subjects exhibited clear and quantifiable deviations from the healthy baseline profile. Chronic metabolic disease (diabetes) resulted in a 62% reduction in crest time gradient, a 72% increase in stiffness index, and reduced HRV, indicating structural vascular impairment. In contrast, acute inflammatory conditions produced a 55% reduction in crest time gradient, a 52% increase in stiffness index, and a 25% reduction in HRV, reflecting transient physiological disturbances. These findings demonstrate that the multi-site PPG framework is sensitive to both structural and functional alterations in cardiovascular dynamics. The ability to detect deviations in spatial pulse gradients provides quantitative support for the Ayurvedic concept of Vikriti as a measurable departure from baseline physiological organization.

V. Discussion

The primary objective of this study was to quantitatively evaluate whether the classical Ayurvedic premise of Nadi Pariksha that the three radial pulse locations corresponding to Vata, Pitta, and Kapha represent

Manuscript received 16 January 2026; Revised 20 March 2026; Accepted 30 March 2026; Available online 1 April 2026
Digital Object Identifier (**DOI**): https://doi.org/10.35882/jeeemi.v8i2.1474

distinct physiological states can be validated through modern cardiovascular signal analysis. Using synchronized multi-site photoplethysmography and a within-subject analytical framework, the results demonstrate clear and statistically significant spatial differentiation across the three pulse locations.

Statistical analysis confirmed significant variation in multiple waveform and autonomic parameters. Crest time showed a significant difference across sites (H= 9.15, p=0.010), with values increasing from 0.175 s at Vata to 0.204s at Kapha, corresponding to an approximate 16.6% increase, indicating slower systolic upstroke and increased vascular damping. Similarly, pulse width at 50% amplitude increased from 0.109s to 0.140s, representing a 28.4% increase, reflecting broader waveform morphology and reduced sharpness. Additional parameters, including systolic amplitude (H =7.82, p=0.020) and systolic area (H=7.54, p=0.023), also demonstrated statistically significant differences, while heart rate variability showed a significant reduction across sites (SDNN: H=6.33, p=0.041). SDNN decreased from 21.03ms at the Vata site to 9.04ms at the Kapha site, corresponding to a 57% reduction, indicating progressively reduced autonomic variability. The observed effect sizes (η^2=0.12-0.20) indicate moderate-to-large physiological effects rather than marginal statistical differences.

Pairwise comparisons further highlighted that the strongest differentiation occurred between the Vata and Kapha pulse locations. Significant differences were observed for crest time (p=0.004) and systolic width (p= 0.001), with corresponding effect sizes of 0.55 and 0.63, respectively, indicating meaningful physiological separation. In contrast, differences between Pitta and Kapha were comparatively smaller and often non-significant, supporting the presence of a physiological continuum rather than discrete segmentation. The Pitta pulse site consistently exhibited intermediate characteristics. For example, crest time at Pitta (0.198s) lies between Vata (0.175s) and Kapha (0.204s), while HRV parameters such as SDNN (12.08 ms) also fall between the higher variability of Vata and lower variability of Kapha. This graded pattern suggests that the radial artery exhibits a continuous physiological transition rather than independent pulse signatures, aligning with the Ayurvedic concept of Pitta as a regulatory state balancing Vata and Kapha dynamics.

An important observation is the coupling between waveform morphology and autonomic variability. The Vata site demonstrated both faster waveform dynamics and higher HRV (SDNN=21.03ms; RMSSD=19.34ms), whereas the Kapha site exhibited slower waveform dynamics and reduced variability (SDNN=9.04ms; RMSSD=7.88ms). This corresponds to an approximate 57% reduction in SDNN and 59% reduction in RMSSD, indicating that vascular dynamics and autonomic regulation are physiologically linked. These findings suggest that pulse waveform morphology is not solely determined by vascular mechanics but is also influenced by neurocardiac modulation.

The clinical analysis further supports the sensitivity of the proposed framework in detecting pathological deviations. In the diabetic subject, the Vata-Kapha crest time gradient decreased from 29ms to 11ms, representing a 62.1% reduction, while the stiffness index increased from 2050 to 3531, corresponding to a 72.2% increase. These changes indicate significant arterial stiffening and reduced spatial pulse differentiation, consistent with known vascular complications of diabetes. In contrast, the acute infection case exhibited a crest time gradient reduction from 29ms to 13ms, corresponding to a 55.2% decrease, along with a 52.6% increase in stiffness index and a 25% reduction in SDNN. These changes suggest transient alterations in vascular tone and autonomic balance rather than structural vascular remodeling. The distinction between chronic and acute conditions highlights the ability of the multi-site framework to differentiate between long-term pathological changes and temporary physiological perturbations. Previous studies on multi-point radial pulse acquisition, particularly PPG-based approaches, have primarily demonstrated strong inter-sensor coupling with high cross-correlation values ($r \approx 0.75$-0.95) and relatively small temporal delays in the range of 5-12ms as shown in Table 7, indicating that adjacent pulse signals largely reflect common mechanical propagation phenomena along the arterial wall. In contrast, the present study demonstrates substantially larger spatial variations, with crest time differences reaching 29ms and relative changes of 16.6%, and pulse width variations of up to 28.4%. These values exceed typical variation ranges (10-20%) reported in flexible multi-sensor pulse systems, suggesting that the observed differences are not merely due to measurement noise or mechanical propagation, but represent structured physiological gradients along the radial artery.

Furthermore, unlike prior studies that focus primarily on classification accuracy (typically 85-93%) or signal fusion, the present work incorporates within-subject statistical validation and effect size analysis, revealing moderate-to-large effects (η^2 = 0.12-0.20). The integration of heart rate variability further demonstrates substantial autonomic variation across pulse sites, with SDNN differences reaching up to 57%, which has not been reported in earlier multi-point pulse studies. Collectively, these findings indicate that multi-site pulse signals are not only mechanically coupled but also

Manuscript received 16 January 2026; Revised 20 March 2026; Accepted 30 March 2026; Available online 1 April 2026
Digital Object Identifier (**DOI**): https://doi.org/10.35882/jeeemi.v8i2.1474

Table 7. Comparison with Related Studies

Study	Sensor Type	Multi-Site	Within-Subject Statistical Testing	Key Quantitative Findings	Effect Size	Clinical Validation
Storchun et al. (PPG Radial Artery)	Pressure sensors	Yes	Yes (limited)	Time delay: 5-12 ms, Correlation: 0.75-0.95	Not reported	No
Wang et al. (Multichannel Fusion)	Pressure sensors	Yes	No	Classification accuracy: ~85-90%	Not reported	No
Jiang et al. (Feature Fusion)	Multi-channel pulse	Yes	No	Accuracy: ~88-93%	Not reported	No
Flexible Sensor Study (2021)	Flexible multi-point sensor	Yes	No	Signal variation: ~10-20%	Not reported	No
Charlton et al. (PPG HRV)	Wearable PPG	No	Limited	HRV error: ~5-10%	Not reported	No
Present Study	Multi-site synchronized PPG	Yes	Yes (paired t-test + KW)	Crest time: 16.6%, Pulse width: 28.4%, SDNN: 57%	η^2 = 0.12-0.20	Preliminary (n=7)

encode physiologically distinct information, supporting the hypothesis of functional heterogeneity across radial artery locations. Unlike prior multi-point pulse studies that report small temporal differences (5-12ms) and high signal correlation, the present study demonstrates significantly larger spatial gradients (up to 29ms and 57% variation) with moderate to large effect sizes, indicating physiologically meaningful differentiation rather than simple mechanical propagation.

Despite these findings, certain limitations must be acknowledged. The number of clinically characterized subjects was limited (n=7), which restricts the generalizability of disease related observations. Additionally, although sensor placement was standardized using an ergonomic fixture, direct measurement of contact pressure was not implemented, which may introduce minor variability. Furthermore, the analysis was limited to time-domain HRV and morphological features; inclusion of spectral or nonlinear metrics could provide additional insights. From a broader perspective, these findings have important implications for the standardization of digital Nadi Pariksha. The results indicate that synchronized multi-site acquisition is essential for capturing spatial pulse gradients, while integration of HRV and morphological features provides a comprehensive representation of cardiovascular dynamics. Establishing normative thresholds for parameters such as crest time gradients, pulse width, and HRV variability may enable objective detection of physiological imbalance.

Overall, the results demonstrate that the classical Vata-Pitta-Kapha pulse model corresponds to measurable physiological variation along the radial artery. The combination of statistically significant differences, moderate-to-large effect sizes, and clinically meaningful deviations supports the use of multi-site PPG analysis as a quantitative and reproducible framework for digital Nadi Pariksha.

VI. Conclusion

This study quantitatively investigated the classical Ayurvedic premise of Nadi Pariksha that the three radial pulse locations corresponding to Vata, Pitta, and Kapha represent distinct physiological states along the radial artery, using synchronized multi-site photoplethysmography and within-subject statistical analysis. Significant spatial differentiation was observed across pulse sites, particularly in crest time ($H=9.15$, $p=0.010$), pulse width ($H=8.43$, $p=0.015$), systolic amplitude ($H=7.82$, $p=0.020$), systolic area ($H=7.54$, $p=0.023$), and HRV (SDNN: $H=6.33$, $p=0.041$), with moderate-to-large effect sizes ($\eta^2=0.12$-0.20). The strongest contrast occurred between Vata and Kapha, where crest time increased from 0.175s to 0.204s and systolic width from 0.109s to 0.140s, indicating a transition from faster, more variable waveforms to broader and more damped pulse characteristics. Additional findings showed that the Pitta site consistently exhibited intermediate behaviour, supporting a physiological continuum. Preliminary clinical observations from a limited cohort of clinically characterized subjects indicated that the Vata-Kapha

Manuscript received 16 January 2026; Revised 20 March 2026; Accepted 30 March 2026; Available online 1 April 2026
Digital Object Identifier (**DOI**): https://doi.org/10.35882/jeeemi.v8i2.1474

crest time gradient decreased by approximately 62% in diabetes (29ms to 11ms) with a corresponding increase in stiffness index (2050 to 3531), while acute infection showed a 55% reduction in gradient and a 25% decrease in HRV, suggesting disruption of normal pulse dynamics. Future research should prioritize larger and more diverse clinical cohorts, incorporation of additional cardiovascular biomarkers, and multi-center validation to establish a robust and standardized framework for digital Nadi Pariksha.

Acknowledgment

The authors would like to express sincere gratitude to Parul University for the invaluable support and resources provided throughout this research. The facilities, academic environment and encouragement from faculty members have significantly contributed to the completion of this work. This study would not have been possible without the institution's commitment to advancing research and innovation in the field of medical electronics.

Funding

This research received no specific grant from any funding agency in the public, commercial, or not for profit sectors.

Data Availability

Datasets were generated or analyzed during the current study.

Author Contribution

All authors contributed equally to the conception, design, experimentation, data analysis, and manuscript preparation of this study.

Declarations

Ethical Approval

The study involved non-invasive optical pulse measurements with minimal risk and was conducted under institutional research guidelines. Written informed consent was obtained from all participants prior to participation.

Consent for Publication Participants.

Consent for publication was given by all participants

Competing Interests

The authors declare no competing interests.

References

[1] W. Zuo, P. Wang, and D. Zhang, “Comparison of three different types of wrist pulse signals by their physical meanings and diagnosis performance,” *IEEE J. Biomed. Heal. Informatics*, vol. 20, no. 1, pp. 119–127, 2016, doi: 10.1109/JBHI.2014.2369821.

[2] P. H. Charlton *et al.*, “Detecting beats in the photoplethysmogram: Benchmarking open-source algorithms,” *Physiol. Meas.*, vol. 43, no. 8, Aug. 2022, doi: 10.1088/1361-6579/ac826d.

[3] A. J. W. Mathieu *et al.*, “Advanced waveform analysis of the photoplethysmogram signal using complementary signal processing techniques for the extraction of biomarkers of cardiovascular function,” *JRSM Cardiovasc. Dis.*, vol. 13, Jan. 2024, doi: 10.1177/20480040231225384.

[4] C. W. Chang, K. meng Liao, Y. T. Chang, S. H. Wang, Y. chun Chen, and G. C. Wang, “The effect of radial pulse spectrum on the risk of major adverse cardiovascular events in patients with type 2 diabetes,” *J. Diabetes Complications*, vol. 33, no. 2, pp. 160–164, Feb. 2019, doi: 10.1016/j.jdiacomp.2018.10.009.

[5] Y. Tiwari and H. S. Dhakad, “Nadi Pariksha: An ancient Ayurvedic method of diagnosis & prediction,” 2022. [Online]. Available: www.jaims.in, https://doi.org/10.1016/j.jaim.2017.10.007

[6] A. Singh, “Traditional development of pulse examination as diagnostic tool in ayurveda,” Oct. 01, 2019, *Informatics Publishing Limited*. doi: 10.18311/jnr/2019/23738.

[7] S. Joshi and P. Bajaj, “Design Development of Portable Vata, Pitta Kapha [VPK] Pulse Detector to Find Prakriti of an Individual using Artificial Neural Network,” in *2021 6th International Conference for Convergence in Technology, I2CT 2021*, Institute of Electrical and Electronics Engineers Inc., Apr. 2021. doi: 10.1109/I2CT51068.2021.9418155.

[8] P. V. G. Kumar, S. Deshpande, and H. R. Nagendra, “Traditional practices and recent advances in Nadi Pariksha: A comprehensive review,” *J. Ayurveda Integr. Med.*, vol. 10, no. 4, pp. 308–315, Oct. 2019, doi: 10.1016/j.jaim.2017.10.007.

[9] P. Kakria, N. K. Tripathi, and P. Kitipawang, “A real-time health monitoring system for remote cardiac patients using smartphone and wearable sensors,” *Int. J. Telemed. Appl.*, vol. 2015, 2015, doi: 10.1155/2015/373474.

[10] A. Joshi, A. Kulkarni, S. Chandran, V. K. Jayaraman, and B. D. Kulkarni, “Nadi Tarangini: A Pulse Based Diagnostic System,” in *2007 29th Annual International Conference of the IEEE Engineering in Medicine and Biology Society*, IEEE, Aug. 2007, pp. 2207–2210. doi: 10.1109/IEMBS.2007.4352762.

Manuscript received 16 January 2026; Revised 20 March 2026; Accepted 30 March 2026; Available online 1 April 2026
Digital Object Identifier (**DOI**): https://doi.org/10.35882/jeeemi.v8i2.1474

[11] P. Shende, "Wrist Pulse Acquisition and Recording System in Ayurveda for Detection of Prakriti of Person," *Int. J. Res. Eng. Appl. Manag.*, vol. 06, p. 5, 2020, https://doi.org/10.35291/2454-9150.2020.0557.

[12] Z. Zhang, Y. Zhang, L. Yao, H. Song, and A. Kos, "A sensor-based wrist pulse signal processing and lung cancer recognition," *J. Biomed. Inform.*, vol. 79, pp. 107–116, Mar. 2018, doi: 10.1016/j.jbi.2018.01.009.

[13] Á. Solé Morillo, J. Lambert Cause, V. E. Baciu, B. da Silva, J. C. Garcia-Naranjo, and J. Stiens, "PPG EduKit: An Adjustable Photoplethysmography Evaluation System for Educational Activities," *Sensors*, vol. 22, no. 4, Feb. 2022, doi: 10.3390/s22041389.

[14] X. Shilei, H. Zhao, A. Ying, and H. Kun, "The Research of Three Regions Acquisition and Analysis System of Pulse Based on Flexible Sensor," in *E3S Web of Conferences*, EDP Sciences, Jun. 2021. DOI:10.1051/e3sconf/202127103056.

[15] N. Kumar, N. Gouri, and K. B. Ramesh, "A Modern Approach to an Ancient Practice of Nadi Pareeksha Design of Radial Artery Pulse Sensor System View project A Modern Approach to an Ancient Practice of Nadi Pareeksha." [Online]. Available: https://www.researchgate.net/publication/351901000

[16] S. Williamson *et al.*, "Characterising the Photoplethysmography Pulse Waveform for Use in Human Neuroscience: The Hybrid Excess and Decay (HED) Model," Aug. 19, 2021. doi: 10.1101/2021.08.19.456935.

[17] P. Ram Manohar, O. Sorokin, J. Chacko, and V. Nampoothiri, "An exploratory clinical study to determine the utility of heart rate variability analysis in the assessment of dosha imbalance," *J. Ayurveda Integr. Med.*, vol. 9, no. 2, pp. 126–130, Apr. 2018, doi: 10.1016/j.jaim.2017.06.008.

[18] P. Interpretation, "Heart Rate Variability : Standards of Measurement , Physiological Interpretation , and Clinical Use," no. 44, 1996.

[19] S. T. Veerabhadrappa and A. L. Vyas, "Analysis and Classification of Three Trimesters during Normal Pregnancy Using Bispectrum," *IETE J. Res.*, vol. 68, no. 4, pp. 2697–2706, 2022, https://doi.org/10.1080/03772063.2020.1725658.

[20] Y. Chen, L. Zhang, D. Zhang, and D. Zhang, "Wrist pulse signal diagnosis using modified Gaussian models and Fuzzy C-Means classification," *Med. Eng. Phys.*, vol. 31, no. 10, pp. 1283–1289, Dec. 2009, doi: 10.1016/j.medengphy.2009.08.008.

[21] K. Basavaraj and S. Balaji, "Article ID: IJECET_12_03_001 Cite this Article: Kurubara Basavaraj and S Balaji, Nadi Pariksha: A Novel Machine Learning Based Wrist Pulse Analysis through Pulse Auscultation System using K-NN Classifier," *Int. J. Electron. Commun. Eng. Technol.*, vol. 12, no. 3, pp. 1–10, https://doi.org/10.34218/IJECET.12.3.2021.001.

[22] H. Pogadadanda, U. Shwetha Shankar, and K. R. Jansi, "Disease Diagnosis Using Ayurvedic Pulse and Treatment Recommendation Engine," in *2021 7th International Conference on Advanced Computing and Communication Systems, ICACCS 2021*, Institute of Electrical and Electronics Engineers Inc., Mar. 2021, pp. 1254–1258. https://doi.org/10.1109/ICACCS51430.2021.9441843.

[23] D. Wang, D. Zhang, and G. Lu, "An Optimal Pulse System Design by Multichannel Sensors Fusion," *IEEE J. Biomed. Heal. Informatics*, vol. 20, no. 2, pp. 450–459, Mar. 2016, https://doi.org/10.1109/jbhi.2015.2392132.

[24] Q. Zhang, J. Zhou, and B. Zhang, "Graph Based Multichannel Feature Fusion for Wrist Pulse Diagnosis," *IEEE J. Biomed. Heal. Informatics*, vol. 25, no. 10, pp. 3732–3743, Oct. 2021, https://doi.org/10.1109/jbhi.2020.3045274.

[25] R. R. Joshi, "A Biostatistical Approach to Ayurveda: Quantifying the Tridosha," 2004. [Online]. Available: www.ayurvedahc.com/aytest.htm

[26] K. C. Lan, G. Litscher, and T. H. Hung, "Traditional chinese medicine pulse diagnosis on a smartphone using skin impedance at acupoints: A feasibility study," *Sensors (Switzerland)*, vol. 20, no. 16, pp. 1–14, Aug. 2020, https://doi.org/10.3390/s20164618.

[27] B. Thakker, A. Lal Vyas, and D. Mani Tripathi, "Time and frequency domain analysis of wrist pulse signals for health diagnosis", Int. J. Bio. Eng. and Tech., vol. 15, no. 03, 2014.

[28] R. R. Joshi, "Diagnostics using computational nadi patterns," *Math. Comput. Model.*, vol. 41, no. 1, pp. 33–47, Jan. 2005, https://doi.org/10.1016/j.mcm.2004.05.002.

[29] B. Thakker and A. Lal Vyas, "Support Vector Machine for Abnormal Pulse Classification," *Int. J. Comput. Appl.*, vol. 22, no. 7, pp. 13–19, May 2011, https://doi.org/10.5120/2597-3610.

[30] Roopini N, Dr. Joshi Manisha Shivaram, and Dr. Shridhar, "Design Development of a System for Nadi Pariksha," *Int. J. Eng. Res.*, vol. V4, no. 06, Jun. 2015, https://doi.org/10.17577/IJERTV4IS060509.

[31] A. S. Prasad and A. Katti, "Utility of Medical

Manuscript received 16 January 2026; Revised 20 March 2026; Accepted 30 March 2026; Available online 1 April 2026
Digital Object Identifier (**DOI**): https://doi.org/10.35882/jeeemi.v8i2.1474

Instruments in Nadi Pareeksha: A Critical Review," *Int. Res. J. Ayurveda Yoga*, vol. 05, no. 02, pp. 184–187, 2022, https://doi.org/10.47223/IRJAY.2022.5233.

[32] A. A. Fedotov, "Techniques for the Morphological Analysis of the Pulse Wave," *Biomed. Eng. (NY).*, vol. 53, no. 4, pp. 270–274, Nov. 2019, http://dx.doi.org/10.18287/JBPE25.11.020310.

[33] J. Pan, L. Liang, Y. Liang, Q. Tang, and Z. Chen, "Robust modelling of arterial blood pressure reconstruction from photoplethysmography," pp. 1–13, 2024, DOI:10.1038/s41598-024-82026-1.

[34] P. Renevey, R. Vetter, J. Krauss, P. Celka, and Y. Depeursinge, "Wrist-located pulse detection using IR signals, activity and nonlinear artifact cancellation," in *2001 Conference Proceedings of the 23rd Annual International Conference of the IEEE Engineering in Medicine and Biology Society*, IEEE, pp. 3030–3033. https://doi.org/10.1109/IEMBS.2001.1017437.

[35] A. A. Fedotov, "A Pulse Wave Monitor with Adaptive Filtering of Motion Artifacts," *Biomed. Eng. (NY).*, vol. 53, no. 6, pp. 375–379, Mar. 2020, https://doi.org/10.1007/s10527-020-09946-w.

[36] Z. Jiang, C. Guo, J. Zang, G. Lu, and D. Zhang, "Features fusion of multichannel wrist pulse signal based on KL-MGDCCA and decision level combination," *Biomed. Signal Process. Control*, vol. 57, Mar. 2020, https://doi.org/10.1016/j.bspc.2019.101751.

[37] L. Liu, W. Zuo, D. Zhang, N. Li, and H. Zhang, "Combination of heterogeneous features for wrist pulse blood flow signal diagnosis via multiple kernel learning," *IEEE Trans. Inf. Technol. Biomed.*, vol. 16, no. 4, pp. 598–606, 2012, https://doi.org/10.1109/titb.2012.2195188.

[38] L. Tcrt and V. Telefunken, "Reflective Optical Sensor with Transistor Output TCRT5000 (L)," vol. 5000, no. 83760, pp. 1–8.

[39] J. A. Behar *et al.*, "PhysioZoo: The Open Digital Physiological Biomarkers Resource," Sep. 2023, [Online]. Available: http://arxiv.org/abs/2309.04498.

[40] M. I. Goda, P. H. Charlton, and J. A. Behar, "pyPPG: a Python toolbox for comprehensive photoplethysmography signal analysis," *Physiol. Meas.*, vol. 45, no. 4, Apr. 2024, 10.1088/1361-6579/ad33a2, https://dx.doi.org/10.1088/1361-6579/AD33A2.

[41] E. Finnegan, S. Davidson, M. Harford, P. Watkinson, L. Tarassenko, and M. Villarroel, "Features from the photoplethysmogram and the electrocardiogram for estimating changes in blood pressure," *Sci. Rep.*, no. 0123456789, pp. 1–20, 2023, https://doi.org/10.1038/s41598-022-27170-2.

[42] J. Park, H. S. Seok, S. Kim, and H. Shin, "Photoplethysmogram Analysis and Applications : An Integrative Review," vol. 12, no. March, pp. 1–23, 2022, https://doi.org/10.3389/fphys.2021.808451.

[43] Y. V. Storchun, Y. I. Yakovenko, and V. V. Boronoev, "Research of Pulse Signals Mutual Influence in Polysphygmography of Radiary Arteries," *Radioelectron. Commun. Syst.*, vol. 63, no. 8, pp. 441–447, Aug. 2020, https://doi.org/10.3103/S0735272720080063.

Author Biography

Devendra Patel received the B.E. degree in Electronics and Communication Engineering in 2006 from Veer Narmad South Gujarat University and the M.E. degree in Electronics and Communication Engineering in 2013 from Gujarat Technological University, India. He is currently serving as an Assistant Professor at Government Engineering College Bharuch, Gujarat, India. His teaching and research activities focus on biomedical signal processing, embedded systems and sensor-based healthcare technologies. His current research interests include wrist pulse analysis, photoplethysmography signal processing, cardiovascular biomarker extraction, and digital health monitoring systems. He has actively contributed to several interdisciplinary research projects aimed at integrating traditional Ayurvedic diagnostic concepts with modern biomedical sensing and data analysis techniques.

Dr. Mitul Patel received the B.E. degree in Electronics and Communication Engineering from Gujarat University in 2009 and the M.Tech. degree in Electronics and Communication System from Dharamsinh Desai University in 2011. He obtained his Ph.D. degree from Parul University in 2022. He is currently working as an Assistant Professor at the Faculty of Engineering and Technology, Parul University, Vadodara, India. His research interests include biomedical signal processing, Computer vision and intelligent healthcare systems with help of machine learning and deep learning. He has published multiple research papers in international journals and conferences and is actively engaged in applying artificial intelligence techniques to biomedical and healthcare engineering.

Manuscript received 16 January 2026; Revised 20 March 2026; Accepted 30 March 2026; Available online 1 April 2026
Digital Object Identifier (**DOI**): https://doi.org/10.35882/jeeemi.v8i2.1474